Molecular Cell, Volume *83*

Supplemental information

Concerted structural rearrangements enable RNA channeling into the cytoplasmic Ski238-Ski7-exosome assembly

Achim Keidel, Alexander Kögel, Peter Reichelt, Eva Kowalinski, Ingmar B. Schäfer, and Elena Conti

Supplemental Information

Table S1. Cryo electron microscopy data collection summary, processing statistics and model quality indicators (related to Figure 1, 2 and 5)

Data collection parameters and processing					
Dataset	**$Ski238_{FL}$**	**$Ski2_{\Delta Arch}387\text{-}Ski7_N$**			**$Ski238\text{-}Ski7_N\text{-}Exo10$**
Microscope	FEI Titan Krios G2				
Voltage [kV]	300				
Camera	Gatan K3				
Energy Filter	Gatan Quantum-LS (GIF)				
Magnification	105000x	105000x			105000x
Pixel Size [Å]	0.8512	0.8512			0.8512
Electron exposure [$e^-/Å^2$]	67.5	77.7			63.36
Target defocus range [µm]	0.6 – 2.2	0.6 – 2.2			0.6 – 2.2
Number of movies	9416	7127			18608
Initially selected particles	2 023 469	1 017 173			10 437 666
		‘closed’	‘intermediate’	‘open’ Ski3N subtracted	
Final number of particles	385414	371 916	104 956	357690	338 757
Resolution [Å]	2.84	2.84	3.12	2.80	2.55
Local resolution range [Å]	2.84-10				
Sharpening B-factor [$Å^2$]	-121.9	-123.6	-113.5	-117.4	-166.05
Refinement					
No. of atoms	20921	17457	-	11424	30807
Residues (protein/nucleotide)	2790/4	2326/4	-	1506/0	3918/34
Ligands	-	-	-	-	ATP
CC_{box}, CC_{mask}, CC_{volume}	0.69, 0.84, 0.82	0.62, 0.76, 0.75	-	0.61, 0.76, 0.75	0.77, 0.90, 0.86

CC for individual chains (Ski2=A, Ski3=B, Ski8=C,D, Ski7=E, RNA=X	A = 0.776, B = 0.769, C = 0.822, D = 0.767, X= 0.568	A = 0.722, B = 0.676, C = 0.761, D = 0.635, E = 0.592, X = 0.622	-	A = 0.625, B = 0.679, C = 0.770, D = 0.703, E = 0.650	-
Resolution $_{\text{FSC map vs. model (0/0.143/0.5)}}$ [Å]	2.7/2.8/3.0	2.8/2.8/3.1	-	2.7/2.8/3.1	2.4/2.5/2.6
r.m.s. deviations					
Bond legths [Å]	0.002	0.003	-	0.002	0.003
Bond angles [°]	0.452	0.460	-	0.446	0.529
Ramachandran favored [%]	98.15	97.45	-	97.54	96.26
Ramachandran allowed [%]	1.85	2.55	-	2.46	3.74
Ramachandran outliers [%]	0.00	0.00	-	0.00	0.00
MolProbity score	1.12	1.31	-	1.20	1.37
Clash score	3.29	4.15	-	3.10	3.23
Rotamere outliers [%]	0.00	0.00	-	0.00	0.12

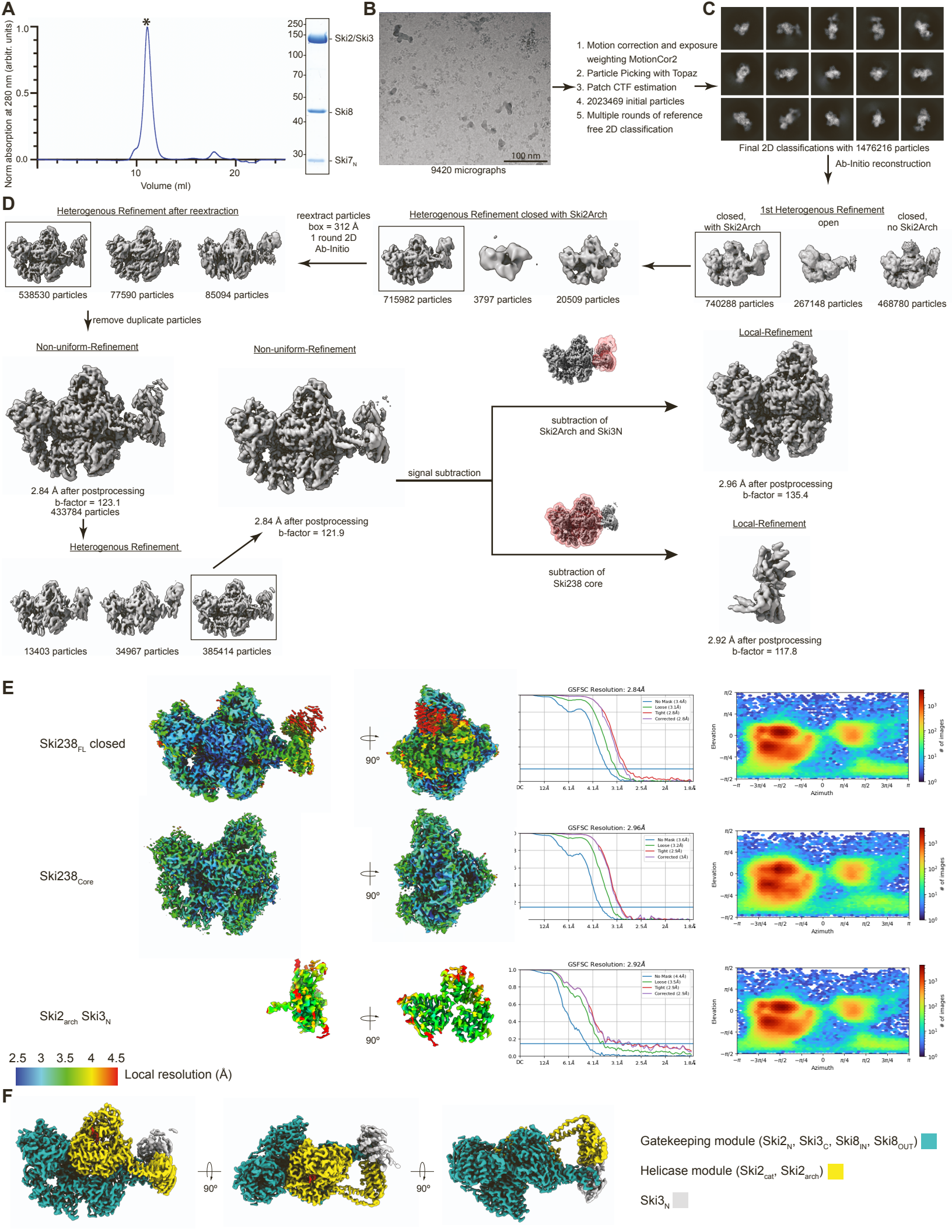
A
Norm absorption at 280 nm (arbitr. units)
Volume (ml)
Ski2/Ski3
Ski8
Ski7N
B
100 nm
9420 micrographs
1. Motion correction and exposure weighting MotionCor2
2. Particle Picking with Topaz
3. Patch CTF estimation
4. 2023469 initial particles
5. Multiple rounds of reference free 2D classification
C
Final 2D classifications with 1476216 particles
Ab-Initio reconstruction
D
Heterogenous Refinement after reextraction
538530 particles
77590 particles
85094 particles
reextract particles
box = 312 Å
1 round 2D
Ab-Initio
Heterogenous Refinement closed with Ski2Arch
715982 particles
3797 particles
20509 particles
1st Heterogenous Refinement
closed, with Ski2Arch
open
closed, no Ski2Arch
740288 particles
267148 particles
468780 particles
remove duplicate particles
Non-uniform-Refinement
2.84 Å after postprocessing
b-factor = 123.1
433784 particles
Non-uniform-Refinement
2.84 Å after postprocessing
b-factor = 121.9
signal subtraction
subtraction of Ski2Arch and Ski3N
subtraction of Ski238 core
Local-Refinement
2.96 Å after postprocessing
b-factor = 135.4
Local-Refinement
2.92 Å after postprocessing
b-factor = 117.8
Heterogenous Refinement
13403 particles
34967 particles
385414 particles
E
Ski238FL closed
Ski238Core
Ski2arch Ski3N
90°
GSFSC Resolution: 2.84Å
GSFSC Resolution: 2.96Å
GSFSC Resolution: 2.92Å
No Mask
Loose
Tight
Corrected
Elevation
Azimuth
# of images
2.5 3 3.5 4 4.5
Local resolution (Å)
F
90°
90°
Gatekeeping module (Ski2N, Ski3C, Ski8IN, Ski8OUT)
Helicase module (Ski2cat, Ski2arch)
Ski3N

Figure S1. Cryo-EM analysis of recombinant full-length Ski238 ($Ski238_{FL}$) with $Ski7_N$ and RNA (related to Figure 1)

(A) Size exclusion chromatography (SEC) analytical profile of $Ski238_{FL}$ reconstituted with $Ski7_N$ over a S200i 10/300 GL column (left) with corresponding 12% Coomassie stained SDS-PAGE of the peak fractions (right).

(B) Representative cryo-EM micrograph collected on a Titan Krios G2 at 300 kV with a pixel size of 0.8512 Å/pix using a K3 direct electron detector.

(C) Representative 2D class averages of the initial selection of $Ski238_{FL}$ complexed with $Ski7_N$.

(D) Cryo-EM data processing scheme. Pre-processing steps and heterogeneous refinement resulted in two particle stacks of $Ski238_{FL}$ in the closed and the open conformation, respectively. For the closed state, a 20 Å low-pass filtered map was used for mask generation (transparent red) focusing either on the Ski238 core or $Ski2_{arch}$:$Ski3_N$. Subsequent signal subtraction and local refinement yielded a map of Ski238 core at a resolution of 3.0 Å and Ski2-Arch:Ski3-N at 2.9 Å. All maps shown are unsharpened maps obtained after refinements.

(E) Local resolution estimates of the final non-uniform and local refinements for the cryo-EM SPA datasets in (D), shown in two different orientations related by a 90˚ rotation around a vertical axis (left panel). Corresponding Fourier shell correlation (FSC) curves of respective maps, as well as angular distribution plot obtained from cryoSPARC (right panel).

(F) Single-particle cryo-EM reconstruction of $Ski238_{FL}$ bound to RNA (Figure 1B) shown in three different orientations related by a 90˚ rotation around a horizontal axis. Gatekeeping module consisting of $Ski2_N$, $Ski3_C$, $Ski8_{IN}$ and $Ski8_{OUT}$ colored in sea green. Helicase module consisting of $Ski2_{cat}$ and $Ski2_{arch}$ colored in yellow. $Ski3_N$ colored in grey RNA colored in red.

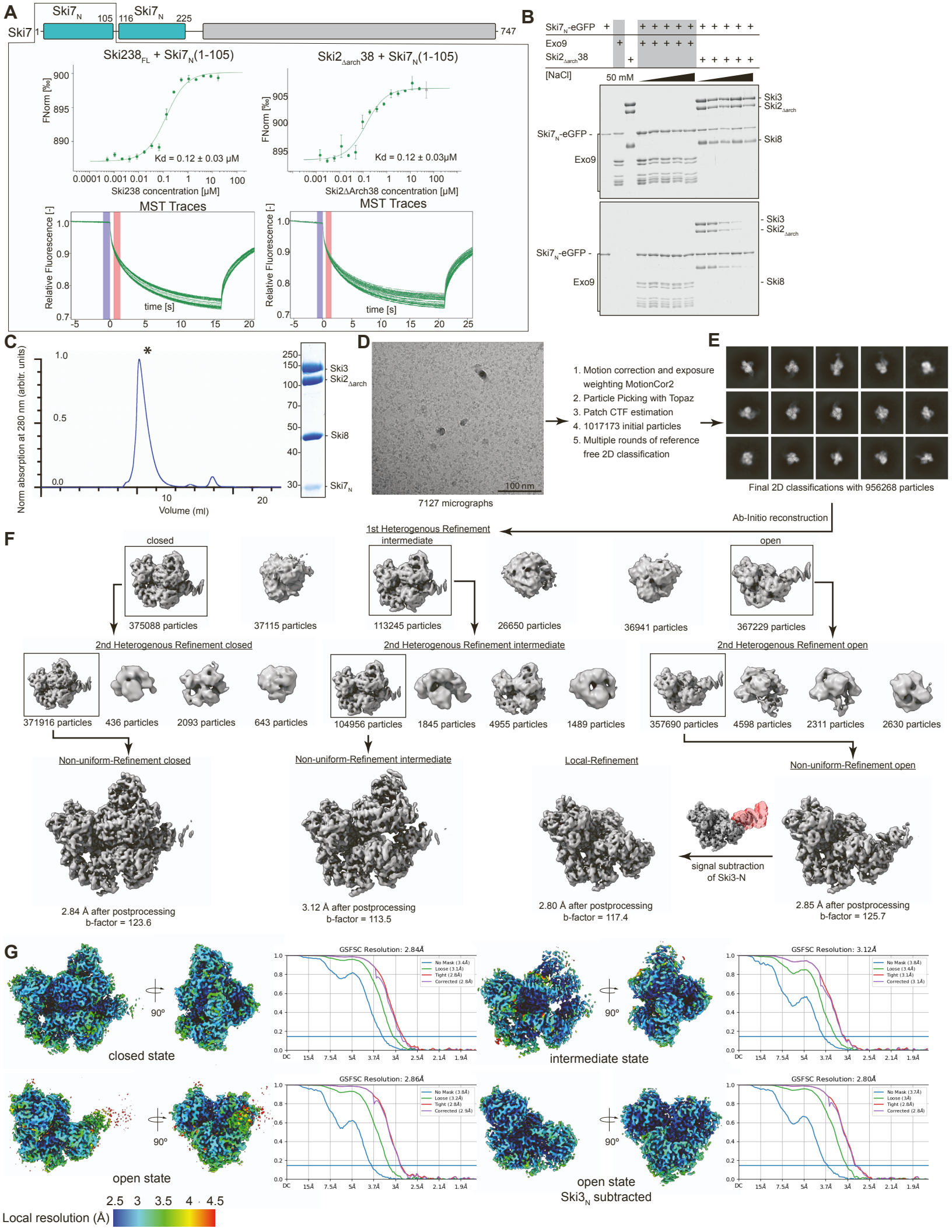
A
Ski7
Ski7N
105
116
Ski7N
225
1
747
Ski238FL + Ski7N(1-105)
FNorm [‰]
Kd = 0.12 ± 0.03 µM
Ski238 concentration [µM]
Ski2Δarch38 + Ski7N(1-105)
Kd = 0.12 ± 0.03µM
Ski2ΔArch38 concentration [µM]
MST Traces
Relative Fluorescence [-]
time [s]
B
Ski7N-eGFP
Exo9
Ski2Δarch38
[NaCl]
50 mM
Ski3
Ski2Δarch
Ski8
C
Norm absorption at 280 nm (arbitr. units)
Volume (ml)
Ski3
Ski2Δarch
Ski8
Ski7N
D
100 nm
7127 micrographs
1. Motion correction and exposure weighting MotionCor2
2. Particle Picking with Topaz
3. Patch CTF estimation
4. 1017173 initial particles
5. Multiple rounds of reference free 2D classification
E
Final 2D classifications with 956268 particles
Ab-Initio reconstruction
F
1st Heterogenous Refinement
closed
intermediate
open
375088 particles
37115 particles
113245 particles
26650 particles
36941 particles
367229 particles
2nd Heterogenous Refinement closed
2nd Heterogenous Refinement intermediate
2nd Heterogenous Refinement open
371916 particles
436 particles
2093 particles
643 particles
104956 particles
1845 particles
4955 particles
1489 particles
357690 particles
4598 particles
2311 particles
2630 particles
Non-uniform-Refinement closed
Non-uniform-Refinement intermediate
Local-Refinement
Non-uniform-Refinement open
2.84 Å after postprocessing
b-factor = 123.6
3.12 Å after postprocessing
b-factor = 113.5
2.80 Å after postprocessing
b-factor = 117.4
signal subtraction of Ski3-N
2.85 Å after postprocessing
b-factor = 125.7
G
90°
closed state
GSFSC Resolution: 2.84Å
GSFSC Resolution: 3.12Å
intermediate state
open state
GSFSC Resolution: 2.86Å
GSFSC Resolution: 2.80Å
open state
Ski3N subtracted
2.5 3 3.5 4 4.5
Local resolution (Å)

Figure S2. Biochemical and structural analysis of Ski2$_{\Delta arch}$38 in complex with Ski7$_N$ (related to Figure 2)

(A) Domain organization of *S. cerevisiae* Ski7 is shown on top, with Ski7$_N$ terminus colored cyan and Ski7-C terminus in gray. The bottom panel shows a biophysical analysis using microscale thermophoresis to quantify the Ski7$_N$ affinity (Ski7$_N$-(1-105)-NHS-Red) for Ski238$_{FL}$ and Ski2$_{\Delta arch}$38. Dissociation constants (K_D) were calculated from triplicate measurements with standard deviation indicated by error bars (Kd 0.12 ± 0.03 μM for both measurements). The respective MST-traces are shown.

(B) Protein coprecipitations with GFP pull-down assays. with recombinant Ski2$_{\Delta arch}$38, Exo9 and Ski7$_N$-(eGFP-Ski7(1-235)-Strep). Increasing salt concentrations (50 mM, 10 mM, 300 mM, 500 mM, 1000mM NaCl) are indicated by black triangles.

(C) SEC analytical profile of recombinant Ski2$_{\Delta arch}$38-Ski7$_N$ reconstituted over a S200i 10/300 GL column (left panel) with corresponding 12% Coomassie stained SDS-PAGE gel of the peak fraction (right panel).

(D) Representative cryo-EM micrograph of Ski2$_{\Delta arch}$38-Ski7$_N$ collected on a Titan Krios G2 at 300 kV with a pixel size of 0.8512 Å/pix using a K3 direct electron detector.

(E) Representative 2D class averages of Ski2$_{\Delta arch}$38-Ski7$_N$.

(F) Cryo-EM data processing scheme. Heterogeneous refinement of 2D class averages resulted in three major particle stacks representing Ski2$_{\Delta arch}$38-Ski7$_N$ in a closed, intermediate and open conformation. Respective particle stacks (black boxes) were used for another round of heterogenous refinement followed by non-uniform refinement of the best resulting class. For the open conformation, a 20 Å low-pass filtered map was used for mask generation (transparent red) focusing on the flexible Ski3$_N$. Subsequent signal subtractions and local refinement yielded a map of open Ski2$_{\Delta arch}$38-Ski7$_N$ at a resolution of 2.8 Å. All maps shown are unsharpened maps obtained after refinements.

(G) Local resolution estimation of the final non-uniform and local refinements for $Ski2_{\Delta arch}38$-$Ski7_{N}$ cryo-EM SPA datasets, with orientations and color scheme same as Figure S1E. Corresponding FSC curves obtained from cryoSPARC.

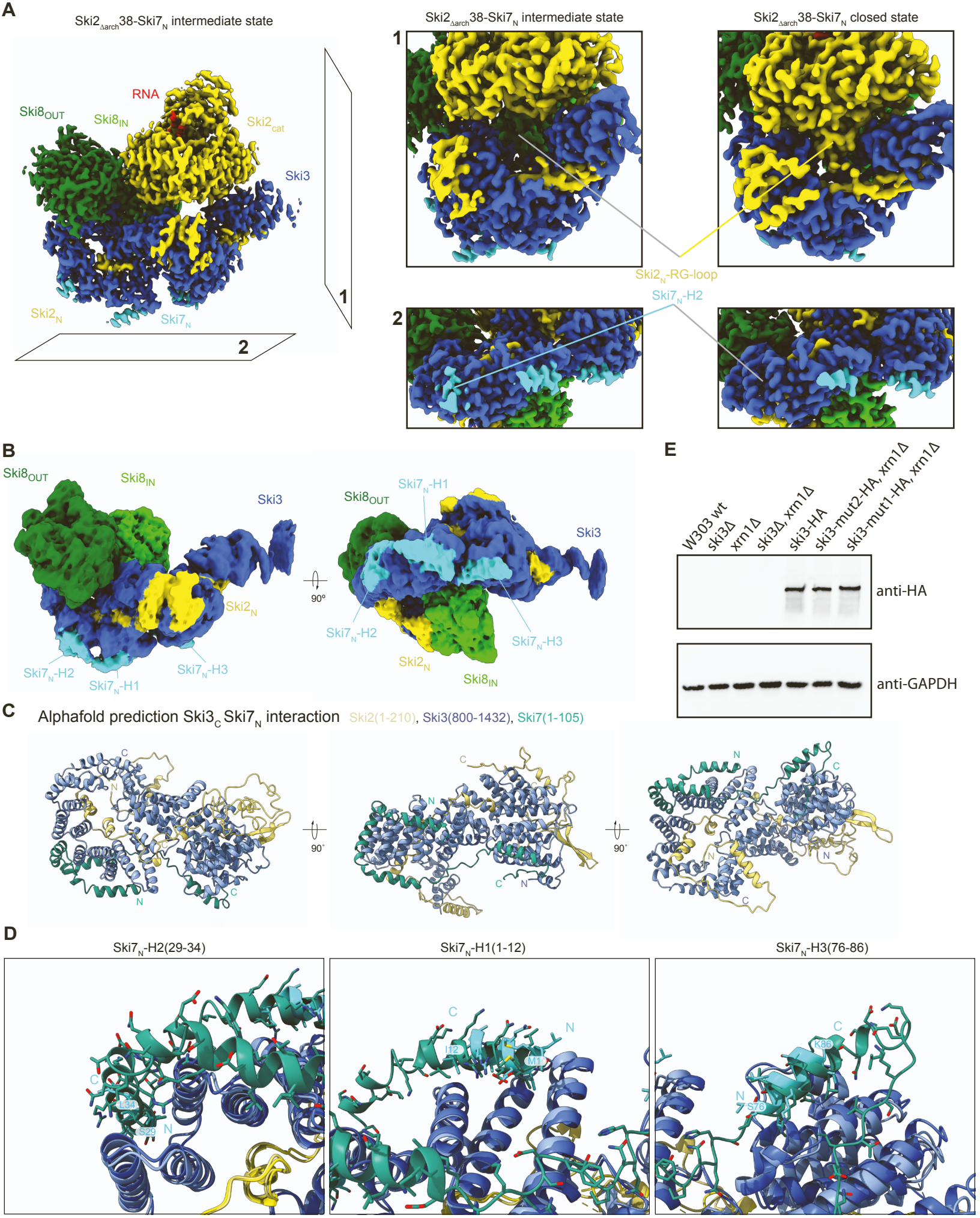
A
Ski2Δarch38-Ski7N intermediate state
RNA
Ski8OUT
Ski8IN
Ski2cat
Ski3
Ski2N
Ski7N
1
2
Ski2Δarch38-Ski7N intermediate state
Ski2Δarch38-Ski7N closed state
Ski2N-RG-loop
Ski7N-H2
B
Ski8OUT
Ski8IN
Ski3
Ski2N
Ski7N-H2
Ski7N-H1
Ski7N-H3
90°
Ski7N-H1
Ski8OUT
Ski3
Ski7N-H2
Ski7N-H3
Ski2N
Ski8IN
E
W303 wt
ski3Δ
xrn1Δ
ski3Δ, xrn1Δ
ski3-HA
ski3-mut2-HA, xrn1Δ
ski3-mut1-HA, xrn1Δ
anti-HA
anti-GAPDH
C
Alphafold prediction Ski3C Ski7N interaction Ski2(1-210), Ski3(800-1432), Ski7(1-105)
90°
90°
D
Ski7N-H2(29-34)
Ski7N-H1(1-12)
Ski7N-H3(76-86)
L34
S29
I12
M1
K86
S76

Figure S3. Map interpretation and model validation of $Ski7_N$ on $Ski2_{\Delta arch}38$ by Alphafold2 predictions (related to Figure 3)

(A) 3D reconstruction of $Ski2_{\Delta arch38}$-$Ski7_N$ in the intermediate conformation (left panel). Colors and orientation are identical to Figure 2A. (1-2) Planes indicate a front view (1) and a bottom view (2) of the complex. Comparison of $Ski2_{\Delta arch}38$-$Ski7_N$ intermediate and closed conformation (right panel). (1) Zoom-in view showing the position of $Ski2_{cat}$ and $Ski2_N$-RG-loop/Wedge (129-164) [27,28]. Note that the RG-loop/Wedge does not adopt a defined structural conformation and that $Ski2_{cat}$ is shifted upwards compared to the closed conformation. (2) Zoom-in view of the $Ski7_N$ binding site on $Ski3_C$ showing that Ski7-H2 is not recruited in the closed state.

(B) Unsharpened 3D reconstructions of $Ski2_{\Delta arch}38$-$Ski7_N$ in open state at low threshold (ChimeraX, level ~ 0.1), shown in two orientations related by a 90˚ rotation around a horizontal axis. Ski2 colored in yellow, Ski3 in blue, $Ski8_{IN}$ in green and $Ski8_{OUT}$ in dark green, and RNA in red. Additional signal in the open state was observed at $Ski3_C$ and assigned to $Ski7_N$ (cyan).

(C) Alphafold2 multimer prediction of the Ski23 in the open conformation and Ski7 binding sites showed overall structural similarity to the cryo-EM map analysis. Ski2-N (1-210) (pale yellow) $Ski3_C$(800-1432) (light blue) and $Ski7_N$ (1-105) (sea green) shown in three different orientations related by a 90˚ rotation around a vertical axis. N and C termini are indicated by N and C and colored according to the corresponding protein.

(D) Superposition of Alphafold2 prediction (C) and the $Ski2_{\Delta arch}38$-$Ski7_N$ model reconstructed in this study. Zoom-in views at $Ski7_N$-H2 (left panel), $Ski7_N$-H1 (middle panel) and $Ski7_N$-H3 (right panel). Colors for the predicted model are identical to (C) and colors for $Ski2_{\Delta arch}38$-$Ski7_N$ are identical to Figure 3B. $Ski7_N$ is in stick representation, with residues indicated.

(E) Western blot of different *S. cerevisiae* Ski3 strains to compare expression level. Different yeast lysates where tested for anit-HA antibody (upper part) and anti-GAPDH antibody (lower part).

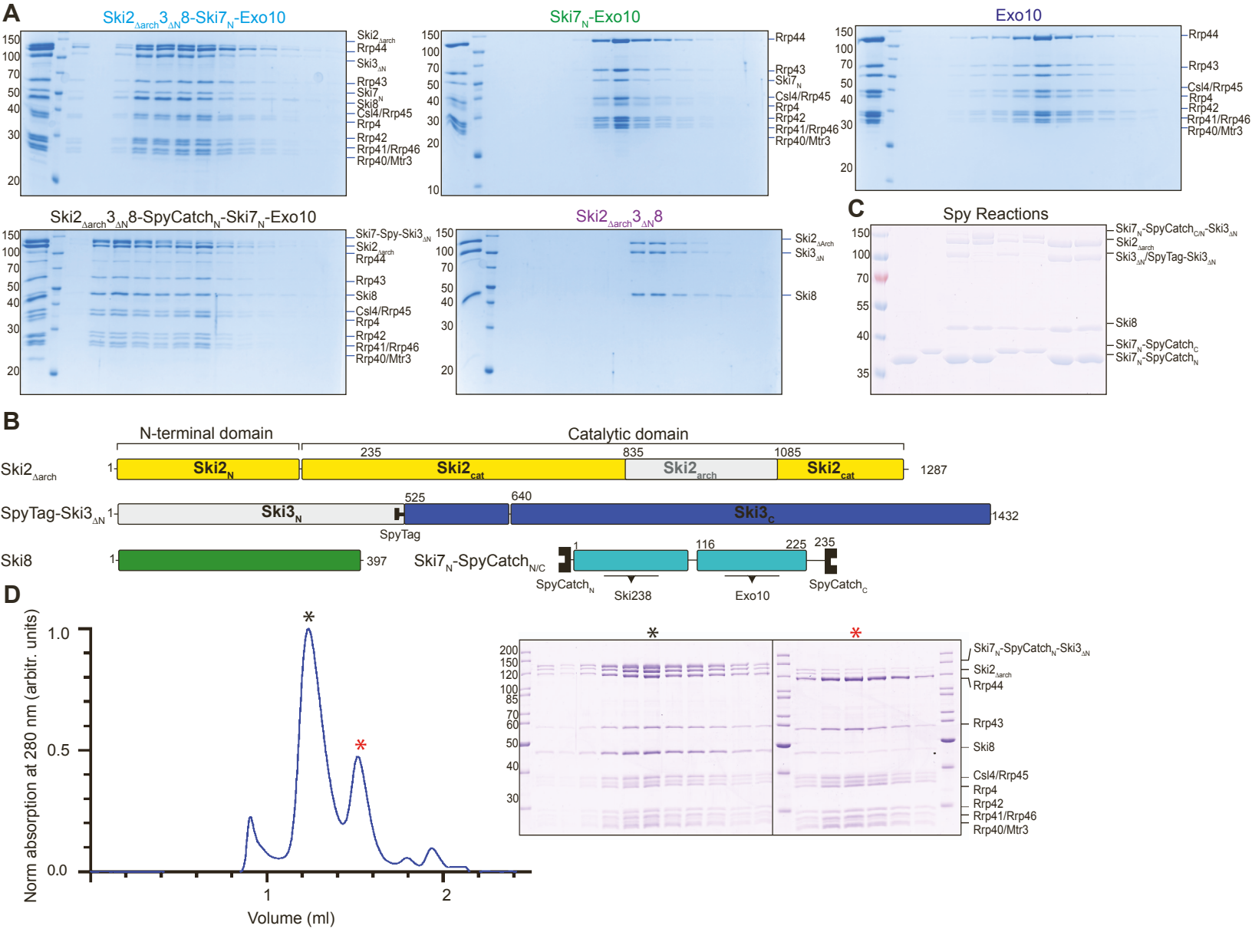
A
Ski2Δarch3ΔN8-Ski7N-Exo10
Ski2Δarch
Rrp44
Ski3ΔN
Rrp43
Ski7N
Ski8
Csl4/Rrp45
Rrp4
Rrp42
Rrp41/Rrp46
Rrp40/Mtr3
Ski7N-Exo10
Rrp44
Rrp43
Ski7N
Csl4/Rrp45
Rrp4
Rrp42
Rrp41/Rrp46
Rrp40/Mtr3
Exo10
Rrp44
Rrp43
Csl4/Rrp45
Rrp4
Rrp42
Rrp41/Rrp46
Rrp40/Mtr3
Ski2Δarch3ΔN8-SpyCatchN-Ski7N-Exo10
Ski7-Spy-Ski3ΔN
Ski2Δarch
Rrp44
Rrp43
Ski8
Csl4/Rrp45
Rrp4
Rrp42
Rrp41/Rrp46
Rrp40/Mtr3
Ski2Δarch3ΔN8
Ski2ΔArch
Ski3ΔN
Ski8
C
Spy Reactions
Ski7N-SpyCatchC/N-Ski3ΔN
Ski2Δarch
Ski3ΔN/SpyTag-Ski3ΔN
Ski8
Ski7N-SpyCatchC
Ski7N-SpyCatchN
B
N-terminal domain
Catalytic domain
Ski2Δarch
Ski2N
Ski2cat
Ski2arch
Ski2cat
1287
SpyTag-Ski3ΔN
Ski3N
Ski3C
1432
SpyTag
Ski8
397
Ski7N-SpyCatchN/C
SpyCatchN
Ski238
Exo10
SpyCatchC
D
Norm absorption at 280 nm (arbitr. units)
Volume (ml)
Ski7N-SpyCatchN-Ski3ΔN
Ski2Δarch
Rrp44
Rrp43
Ski8
Csl4/Rrp45
Rrp4
Rrp42
Rrp41/Rrp46
Rrp40/Mtr3

Figure S4. Biochemical characterization of recombinant Ski238 with $Ski7_N$ and Exo10 (related to Figure 4)

(A) Coomassie-stained 12% SDS-PAGE gels showing protein components from SEC peak fractions after runs with different Exo10, Ski7 and Ski238 combinations. Color of the labels correspond to color of the corresponding curves in Figure 4A.

(B) Domain organization of the yeast $Ski2_{\Delta arch}3_{\Delta N}8$ and $Ski7_N$ showing placement of the SpyTag and SpyCatcher (SpyCatch). Constructs were used for stabilization of Ski238- $Ski7_N$-Exo10 (also see Figure 4B). Ski238 subunits Ski2 (yellow) Ski3 (blue) Ski8 (green) and SpyTag (black). $Ski7_N$ (cyan/grey) and $SpyCatch_{N/C}$ (black). Grey areas represent deleted portions.

(C) SDS-PAGE gel confirming covalent linking between Spy-$Ski2_{\Delta arch}3_{\Delta N}8$ and $SpyCatch_{N/C}$-$Ski7_N$.

(D) Reconstitution of Ski238-$SpyCatch_N$-Ski7 with Exo10 over S6i 3.2/300GL SEC column used for cryo-EM SPA. SEC profile (left panel) with corresponding 12% Coomassie stained SDS-PAGE of the individual fractions (right panel).

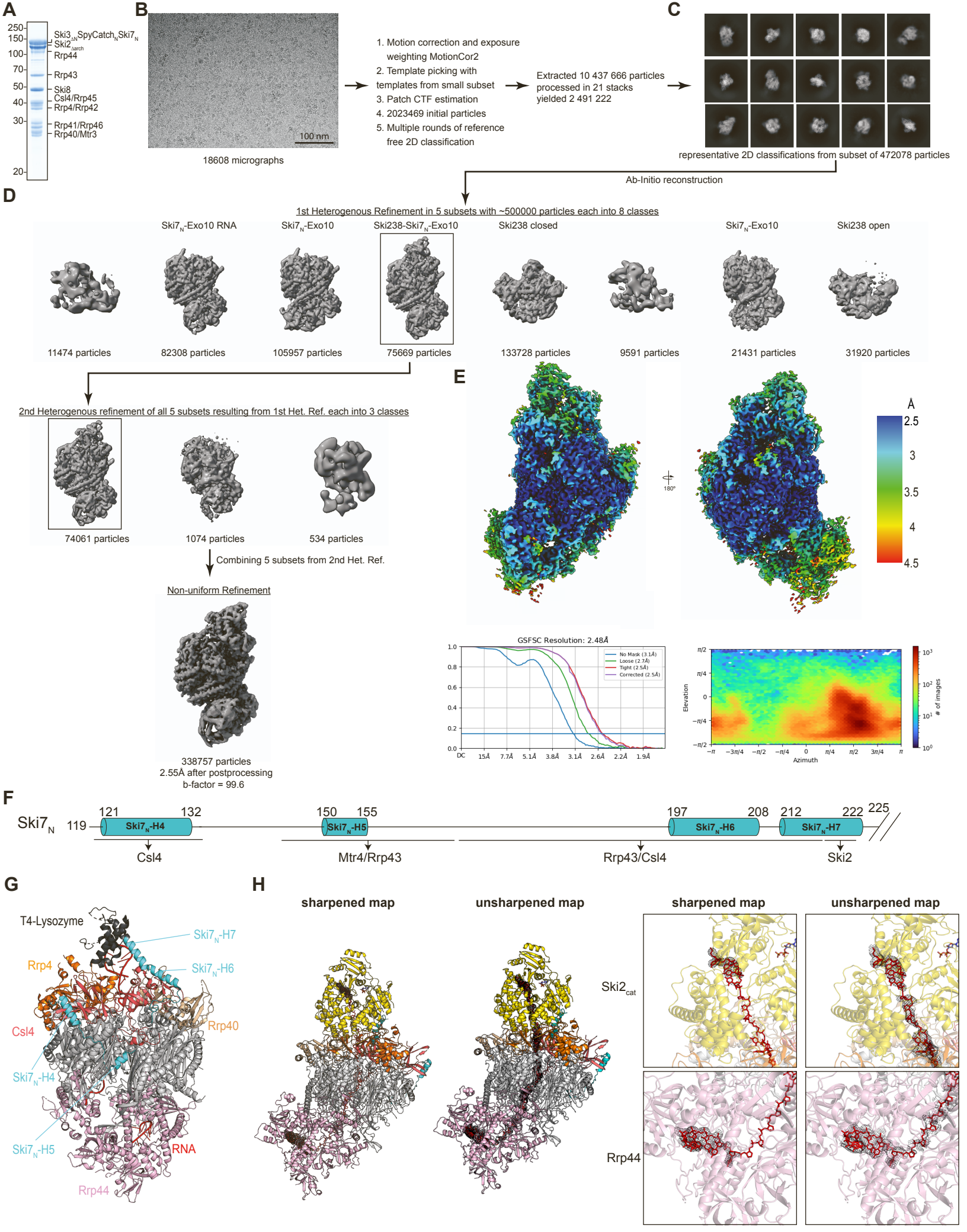
A
250
150
100
70
50
40
30
20
Ski3$_{1N}$SpyCatch$_N$Ski7$_N$
Ski2$_{1arch}$
Rrp44
Rrp43
Ski8
Csl4/Rrp45
Rrp4/Rrp42
Rrp41/Rrp46
Rrp40/Mtr3
B
100 nm
18608 micrographs
1. Motion correction and exposure weighting MotionCor2
2. Template picking with templates from small subset
3. Patch CTF estimation
4. 2023469 initial particles
5. Multiple rounds of reference free 2D classification
Extracted 10 437 666 particles processed in 21 stacks yielded 2 491 222
C
representative 2D classifications from subset of 472078 particles
Ab-Initio reconstruction
D
1st Heterogenous Refinement in 5 subsets with ~500000 particles each into 8 classes
Ski7$_N$-Exo10 RNA
Ski7$_N$-Exo10
Ski238-Ski7$_N$-Exo10
Ski238 closed
Ski7$_N$-Exo10
Ski238 open
11474 particles
82308 particles
105957 particles
75669 particles
133728 particles
9591 particles
21431 particles
31920 particles
2nd Heterogenous refinement of all 5 subsets resulting from 1st Het. Ref. each into 3 classes
74061 particles
1074 particles
534 particles
Combining 5 subsets from 2nd Het. Ref.
Non-uniform Refinement
338757 particles
2.55Å after postprocessing
b-factor = 99.6
E
180°
Å
2.5
3
3.5
4
4.5
GSFSC Resolution: 2.48Å
No Mask (3.1Å)
Loose (2.7Å)
Tight (2.5Å)
Corrected (2.5Å)
DC
15Å
7.7Å
5.1Å
3.8Å
3.1Å
2.6Å
2.2Å
1.9Å
Elevation
Azimuth
# of images
F
Ski7$_N$
119
121
132
150
155
197
208
212
222
225
Ski7$_N$-H4
Ski7$_N$-H5
Ski7$_N$-H6
Ski7$_N$-H7
Csl4
Mtr4/Rrp43
Rrp43/Csl4
Ski2
G
T4-Lysozyme
Ski7$_N$-H7
Rrp4
Ski7$_N$-H6
Rrp40
Csl4
Ski7$_N$-H4
Ski7$_N$-H5
RNA
Rrp44
H
sharpened map
unsharpened map
sharpened map
unsharpened map
Ski2$_{cat}$
Rrp44

Figure S5. Cryo-EM analysis of recombinant active Ski238-Ski7-Exo10 holocomplex (related to Figure 4)

(A) Coomassie-stained 12% SDS-PAGE gel of the SEC peak fraction of Ski238-SpyCatch$_N$-Ski7 with Exo10 after incubation with ATP and RNA (see also Figure S4D).

(B) Representative cryo-EM micrograph collected on a Titan Krios G2 collected at 300 kV with a pixel size of 0.8512 Å/pix using a K3 direct electron.

(C) Representative 2D class averages.

(D) Cryo-EM data processing scheme. After pre-processing steps and 2D classification, selected particles were classified by heterogeneous refinement and 3D classification into five subclasses representing various subcomplexes. The sub-population of particles clearly representing the Ski7$_N$-Exo10 bound to open state Ski238 was subjected to a second round of heterogenous refinement. Afterwards, the obtained particles stacks were merged and subjected to a final non-uniform refinement.

(E) Local resolution estimates of the final non-uniform and local refinements for the cryo-EM SPA datasets in (D), shown in two different orientations related by a 90˚ rotation around a vertical axis (top panel). Corresponding FSC curves of respective map, as well as angular distribution plot obtained from cryoSPARC (bottom panel).

(F) Topology-based domain organization of the Ski7 N-terminal arm (residues 119-225). Secondary structure elements are indicated by cylinders. Interactions between Ski7$_N$ helices with Exo10 subunits and Ski2 are indicated below.

(G) Cartoon representation of *S. cerevisiae* Exo10-Ski7-RNA crystal structure (PDB:5JEA, Kowalinski et al., 2016). Numbering of Ski7 helices have been updated to reflect our findings.

(H) Model of Ski238-Ski7$_N$-Exo10 with RNA density from sharpened (left) and unsharpened (middle) cryo-EM reconstruction shown in black. Orientation and coloring are analog to Figure 5A. Comparison of RNA signal in Ski2$_{cat}$ (upper right) and Rrp44 (lower left). The

unsharpened map shows continuous density for the RNA substrate while the sharpened map only shows density within $Ski2_{cat}$ or Rrp44.

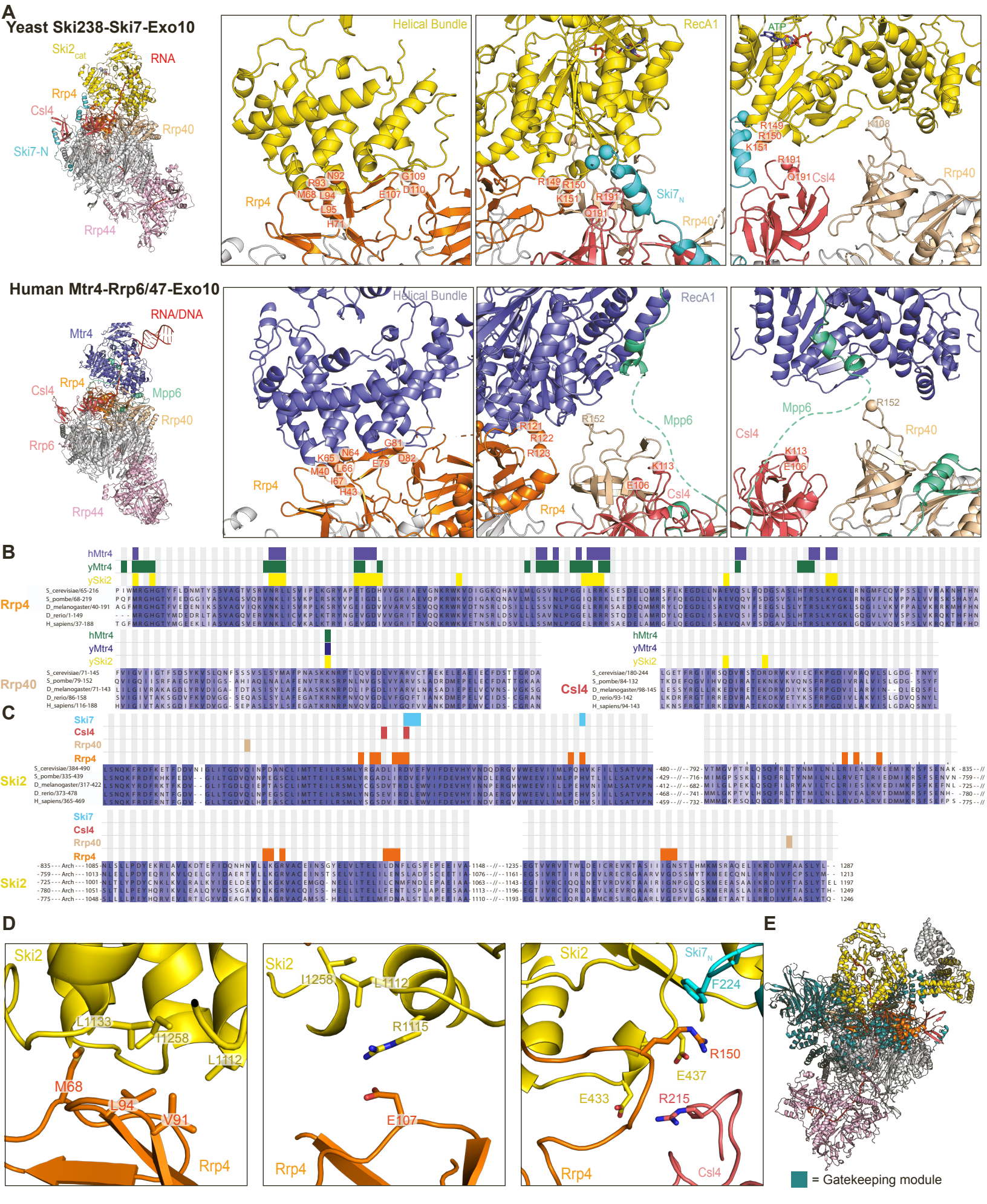
A
Yeast Ski238-Ski7-Exo10
Ski2cat
RNA
Rrp4
Csl4
Rrp40
Ski7-N
Rrp44
Helical Bundle
RecA1
ATP
Rrp4
N92
R93
M68
L94
L95
H71
E107
G109
D110
Ski7N
R149
R150
K151
R191
Q191
K108
Csl4
Human Mtr4-Rrp6/47-Exo10
RNA/DNA
Mtr4
Mpp6
Rrp6
K65
N64
G81
E79
D82
M40
L66
I67
H43
R121
R122
R123
R152
K113
E106
B
hMtr4
yMtr4
ySki2
Rrp4
Rrp40
Csl4
C
Ski7
Csl4
Rrp40
Rrp4
Ski2
D
L1133
I1258
L1112
M68
L94
V91
R1115
E107
F224
R150
E437
E433
R215
E
= Gatekeeping module

Figure S6. Comparison of ySki2 and hMtr4 binding sites on Exo10 with sequence alignments (related to Figure 5)

(A) Comparison of Ski238-Ski7-Exo10 and nuclear exosome helicase assemblies from *S. cerevisiae* (top, this study) and *H. sapiens* (bottom, PDB: 6D6Q), respectively. For both complexes, a model is shown in cartoon representation in the same orientation (left panel). Zoom-in views on the individual binding sites between helicase and the Exo10 cap proteins are shown, similar to Figure 5C and 5D. Conserved residues in cap proteins Csl4, Rrp4 and Rrp40 are shown as spheres and labeled with residue numbers.

(B) Multiple sequence alignments of Exo10 cap proteins from different organisms show conservation of cap proteins and overlap of helicase interaction sites based on available models. (Organism with uniport identifier; *S. cerevisiae*: P17883, *S. pombe*: O94474, *D. melanogaster*: Q6NNB2, *D. rerio*: A0A8M1RLS7, and *H. sapiens*: Q6PGP7). Alignments were performed using Clustal Omega and visualized with Jalview. Sequence conservation is shown by color from variable (white) to conserved (blue). Colored bars above the alignments indicate residues involved in protein-protein interactions with ySki2 (this study), yMtr4 (6FSZ) and hMtr4 (6D6Q).

(C) Amino acid sequence alignments of Ski2 from different organisms. Alignments were performed as above (Figure S6B). Sequence conservation is shown by color from variable (white) to conserved (blue). Residues involved in protein-protein interactions with Rrp4, Rrp40, Csl4 and Ski7 are indicated above the alignment by colored bars.

(D) Close ups on the identified main binding sites between Ski2 and the exosome cap

(E) Superposition of $Ski238_{FL}$ and Ski238-$Ski7_{N}$-Exo10 showing the clash of the Gatekeeping module ($Ski2_{N}$, $Ski3_{C}$, $Ski8_{IN}$, $Ski8_{OUT}$) with the Exo10. Models were superposed on $Ski2_{cat}$. Colors for Ski238-$Ski7_{N}$-Exo10 are identical to Figure 4D. For $Ski238_{FL}$, the Gatekeeping module is colored in sea green. $Ski2_{arch}$ is colored in yellow, $Ski3_{N}$ in grey.